


Electron double-emission spectra for helium atoms in intense 400-nm laser pulses

Jinzhen Zhu and Armin Scrinzi*

Physics Department, Ludwig Maximilians Universität, D-80333 Munich, Germany (Received 20 December 2019; accepted 19 May 2020; published 16 June 2020)

Double photoelectron emission from He atoms by intense laser pulses with a wavelength of 394.5 nm is computed for intensities of $3.5\text{--}9.2 \times 10^{14}$ W/cm². Joint momentum distributions confirm the characteristics seen in classical trajectory calculations. The pronounced transition from back-to-back to side-by-side emission with increasing intensity, the He²⁺/He⁺ ratios, and a modulation of joint energy spectra agree well with a recent experiment [K. Henrichs *et al.*, *Phys. Rev. A* **98**, 043405 (2018)] if one admits an increase in experimental intensities by a factor of ~ 2 . We find that Freeman resonances enhance back-to-back emission, we identify the signature of electron repulsion in joint angular distributions, and we interpret the modulation of joint energy spectra as a signature of multiple recollisions.

DOI: [10.1103/PhysRevA.101.063407](https://doi.org/10.1103/PhysRevA.101.063407)**I. INTRODUCTION**

Double-ionization of noble-gas atoms has been and still is being investigated for studying the effects of elementary correlation and for gauging computational methods. Notably, the measurement of enhanced double ionization by strong laser pulses [1] has triggered a large number of theoretical studies and consensus has emerged that “recollision,” where the first emitted electron collides with the still-bound one, is the primary mechanism of double ionization. Variants of this basic mechanism have been used to explain in increasing detail spectra using short, intense pulses that were obtained by cold-target recoil-ion momentum spectroscopy [2].

The assignment of the observed spectral features to specific mechanisms remains a challenge for theory. The helium atom is, in principle, accessible to a complete numerical solution of its time-dependent Schrödinger equation (TDSE) and the computation of fully differential spectra, even if the parameter range where this can be achieved remains narrow. However, an accurate time-dependent wave function by itself does not provide physical insight or intuitive mechanisms. For that, the use of classical and semiclassical models is of interest. Such models have been very successful in strong-field physics [3–5].

The recollision model for nonsequential double ionization (NSDI) consists of three steps: (1) electron e_1 leaves the atom, typically by tunnel ionization, (2) e_1 picks up energy in the laser field, and (3) it returns to the vicinity of the nucleus, and the second electron e_2 is detached by collision. The scenarios for the interaction in step 3 are often phrased in terms of classical mechanics. Energetic recollisions predominantly occur near nodes of the field. The energy of e_1 , the energy imparted to e_2 , and e_2 's ultimate detachment time are the main parameters to distinguish various classical mechanisms. At large energy, e_1 can knock out e_2 in an $e\text{-}2e$ collision, and the two leave nearly at the same time. When the energy imparted to e_2 is

below the ionization threshold, the simultaneous presence of the laser field can still allow detachment by suppressing the potential barrier. We call the mechanisms where the release occurs within a narrow time window of the recollision “double ionization upon recollision” (DUR), which subsumes direct knockout and release by suppression of the binding barrier as well as tunneling [6–8]. If e_1 loses much of its energy in the process, the field will accelerate both electrons in the same direction, which we denote as side-by-side (SBS) emission. At nonequal energy sharing e_1 continues its path, while e_2 is emitted in the opposite direction, which we call back-to-back (B2B) emission. When studying the momenta, one has to also include scattering of the electrons by the nucleus. Such a process is the “slingshot NSDI” [3], which leads to B2B emission of the two electrons, even when both electrons have comparably low momenta upon recollision.

When an actual excited state is formed with a decay time that is not locked to the recollision event, one speaks of “recollision-induced excitation with subsequent ionization” (RESI) [9,10], which allows both SBS and B2B emissions. A similar pattern where, however, SBS emission is favored is the formation of a quasibound state of both electrons which can survive for at least one quarter cycle and gets ionized with the electrons moving in the same direction (“doubly delayed ejection” [11]).

In this paper we present *ab initio* quantum-mechanical calculations of double ionization of the He atom by short and intense laser pulses at a carrier wavelength of 394.5 nm and relate these to recent measurements and some of the mechanisms listed above. Dependence of SBS and B2B emission on pulse intensity and pulse duration is used as the main observable.

We present joint energy and momentum distributions at various intensities and pulse durations and find generally good agreement with measurement. Our simulations also show enhanced B2B emission at nonequal energy sharing, as predicted by the classical models. B2B emission is further enhanced by Freeman resonances, a genuinely quantum phenomenon. Finally, we will point to another manifestation of quantum

*Armin.Scrinzi@lmu.de

mechanics, namely, the modulation by $2\hbar\omega$ of the joint energy distribution along lines of constant sum energy—the “checkerboard pattern” of Ref. [12]. In classical language this translates into repeated electron collisions. We also present calculations with ultrashort pulses (2 fs FWHM, parameters of Ref. [3]) that generally support the slingshot mechanism of Ref. [3], although the match is found at lower than predicted intensity.

II. METHODS AND LASER PARAMETERS

A. Two-electron calculations

The Hamiltonian of the He atom with infinite nuclear mass is (using atomic units $\hbar = e^2 = m_e = 4\pi\epsilon_0 = 1$, denoted as a.u.)

$$H(\vec{r}_1, \vec{r}_2, t) = H_I(\vec{r}_1, t) + H_I(\vec{r}_2, t) + \frac{1}{|\vec{r}_1 - \vec{r}_2|}, \quad (1)$$

with the ionic Hamiltonian

$$H_I(\vec{r}, t) = -\frac{\Delta}{2} - i\vec{A}(t) \cdot \vec{\nabla} - \frac{2}{r}. \quad (2)$$

Interaction with the laser is described in dipole approximation and velocity gauge, where \vec{A} is defined below.

To numerically solve the TDSE and to compute spectra we use the time-dependent recursive indexing (tRecX) code [13]. tRecX implements the time-dependent surface flux (tSURFF) method [14,15] (see also Refs. [16–22]), infinite-range exterior complex scaling (irECS) [23,24], and the finite-element discrete variable representation (FE-DVR) methods [25]. In brief, the full two-electron calculation is restricted to within a surface radius $|\vec{r}_1|, |\vec{r}_2| \leq R_s$ with irECS absorption beyond R_s . tSURFF is based on the idea that beyond R_s all interactions can be neglected and spectra are reconstructed from the time evolution of values and derivatives on a four-dimensional hypersurface $|\vec{r}_1| = |\vec{r}_2| = R_s$. Expansions into single-particle angular momenta and FE-DVR radial functions are used. The most critical convergence parameters are R_s and, to a lesser degree, the number of angular momenta. All convergence parameters were varied systematically to ensure sufficient accuracy. In the majority of calculations angular momentum quantum numbers $l_i = 0, \dots, 19$ and $|m_i| \leq 1$ were used for each electron. The convergence with R_s was studied using values up to 80 a.u. For the bulk of calculations we found $R_s = 40$ to suffice, except for joint angular distributions, where full convergence requires a simultaneous increase of angular and radial discretization to unreasonable sizes. With that we obtain a He ground-state energy of -2.902 with $|m_i| \leq 1$ and a three-decimal-digit exact value of -2.903 with $|m_i| \leq 2$. In the FE-DVR an 18-point Lobatto quadrature rule was used with an average grid spacing of 0.6 a.u. up to R_s , followed by a 15-point rule for exponentially damped polynomials with complex scaling for absorption. We ensured that for a given R_s the discretization error is negligible on the accuracy level discussed here. Except for the replacement of the exact FE basis with the computationally more efficient FE-DVR grid, the mathematical and numerical background of tRecX and procedures employed to assess convergence are described in full detail in Ref. [22].

As an alternative to extracting single-emission spectra from the full two-electron calculation, we also used a single-active-electron model with the Hamiltonian

$$H_M(t) = -\frac{\Delta}{2} - i\vec{A}(t) \cdot \vec{\nabla} - \frac{1 + e^{-2.135r}}{r}, \quad (3)$$

where the screening factor is chosen to be -2.135 to obtain the ionization potential $I_p = 0.903$ a.u. This simple model largely reproduces results from the full calculation (see below).

B. Differential spectra

Starting from the fully differential momentum spectrum $\sigma(\vec{p}_1, \vec{p}_2)$, we compute various partially differential spectra.

The coplanar joint angular distributions (JADs) at given energy sharing $\eta = (E_1, E_2)$, $E_i = p_i^2/2m_e$ are defined by choosing the first electron at θ_1 and taking into account cylindrical symmetry, i.e.,

$$\sigma_{\text{JAD}}(\theta) = \sigma(p_1, \theta_1, 0, p_2, \theta_2, \varphi_2), \quad (4)$$

with $\varphi_2 = 0$ for $\theta_2 \in [0, \pi]$ and $\varphi_2 = \pi$ for $2\pi - \theta_2 \in [0, \pi]$. For experimentally realistic JADs we average over a small energy region ± 0.3 eV, which is comparable to the spectral width of the pulses used here.

Joint distributions of momentum in the polarization (z) direction and joint energy distributions are defined as

$$\sigma(p_{1z}, p_{2z}) = \int dp_{1x} dp_{2x} dp_{1y} dp_{2y} \sigma(\vec{p}_1, \vec{p}_2), \quad (5)$$

$$\sigma(E_1, E_2) = p_1 p_2 \int d\Omega_1 d\Omega_2 \sigma(\vec{p}_1, \vec{p}_2), \quad (6)$$

where $d\Omega_i$ is the integration over the solid angle of \vec{p}_i . B2B emission is the part of $\sigma(p_{z1}, p_{z2})$ with opposite signs of p_{zi} and SBS with equal signs.

To study correlation in double-electron emission we introduce the correlation ratio Γ of B2B to SBS emission,

$$\Gamma := Y_-/Y_+, \quad (7)$$

$$Y_{\pm} = \iint_0^{\infty} dp_{z1} dp_{z2} [\sigma(p_{z1}, \pm p_{z2}) + \sigma(-p_{z1}, \mp p_{z2})], \quad (8)$$

where larger Γ indicates more B2B emission.

We will further study the correlation at individual energy-sharing points $\eta = (E_1, E_2)$ using the ratio Γ_{η} , where the integration of Y_{\pm} is restricted to a small region surrounding $p_{iz} = \sqrt{2m_e E_i}$, $i = 1, 2$.

C. Laser pulses

The dipole field of a laser pulse with peak intensity $I = \varepsilon_0^2$ (atomic units) and linear polarization in the z direction is defined as $\varepsilon_z(t) = \partial_t A_z(t)$, with

$$A_z(t) = \frac{\varepsilon_0}{\omega} a(t) \sin(\omega t + \varphi_{\text{CEP}}). \quad (9)$$

The wavelength was chosen as exactly $\lambda = 394.5$ nm to match the experimental wavelength used in Ref. [12], with the corresponding photon energy of $\hbar\omega \approx 3.14$ eV. For the pulse envelope $a(t)$ we used two different shapes: a “flat-top” trapezoidal function with a linear rise and descent over a

single optical cycle (1 o.c. = $2\pi/\omega$) and constant amplitude in between. This somewhat unrealistic pulse shape is chosen to better isolate the intensity-dependent effects of Freeman resonances. To examine the robustness and experimental observability of effects we chose $a(t) = [\cos(t/T)]^8$ as a more realistic envelope. Pulse durations are specified by the FWHM with respect to intensity. The carrier-envelope phase φ_{CEP} , in general, affects all nonlinear processes. Highly differential observables such as the JADs show carrier-envelope phase (CEP) dependence for pulses as long as 14 optical cycles. However, yields and energy spectra vary only weakly with φ_{CEP} , reaching observable level only for single- or two-cycle pulses. We compare our results to an experiment with long pulses of FWHM >7 o.c., for which we demonstrate the absence of relevant CEP dependence. Otherwise, unless indicated, calculations are for $\varphi_{\text{CEP}} = 0$.

D. Ponderomotive shifts and Freeman resonances

The ac Stark shifts of ground and excited states differ, leading to intensity-dependent resonance conditions known as Freeman resonances [26]. In good approximation, the shift of excited-state energies relative to the ground state is equal to the ponderomotive potential $U_p = \varepsilon_0^2/(4\omega^2)$, leading to the n -photon Freeman resonance condition

$$-E^{(g)} + E^{(x)} + U_p = n\omega, \quad (10)$$

where $E^{(g)}$ and $E^{(x)}$ are field-free ground- and excited-state energies of the He atom. The validity of this formula for the present purposes was verified by Floquet calculations with the single-electron Hamiltonian (3).

Similarly, photoelectron peaks are shifted to lower energies by U_p as the ponderomotive potential of the continuum electron is not converted into kinetic energy due to the rapid passage of the pulse. The n -photon peaks in single and double emission appear at energies

$$S_n = n\omega - I_p^{(s)} - U_p \quad (11)$$

and

$$D_n = n\omega - I_p^{(d)} - 2U_p, \quad (12)$$

respectively, where $I_p^{(s)}$ and $I_p^{(d)}$ are the ionization potentials for single and double ionization. Note that for the pulse parameters used here, U_p reaches up to several photon energies.

III. SINGLE-ELECTRON EMISSION

In the He atom, single ionization at longer wavelength is little affected by multielectron effects. At 800 nm this was observed for photoemission with linear [22] as well as elliptical polarization [20]. We find the same to hold at the present shorter wavelength. The difference in total yields obtained from the model and full two-electron calculation is about 20%. After normalization, the shapes of the spectra agree within a few percent in the energy range up to 100 eV. As the single-ionization calculation can easily be pushed to complete convergence, this also supports the correctness of the full calculation.

In Fig. 1 we compare the spectral shapes at two sets of intensities, $3.5, 4.6, 5.7 \times 10^{14}$ and $5.7, 7.4, 9.2 \times 10^{14}$ W/cm²,

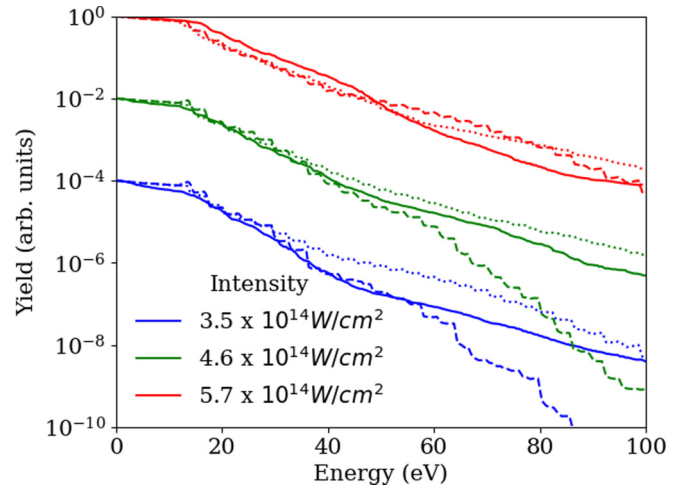


FIG. 1. Single-electron energy spectra. Solid lines: experiment [12]; dashed lines: TDSE; dotted lines: TDSE at intensities of $5.7, 7.4,$ and 9.2×10^{14} W/cm². Curves were smoothed over four photoelectron peaks, normalized, and offset artificially for visibility, descending from the highest intensity on top. The TDSE was solved for a \cos^8 pulse with a duration of 20 fs FWHM. The computed spectra are smoothed over 12 eV for easier comparison with experimental data.

to three measured spectra from Ref. [12]. We verified that on the level of the comparison the exact pulse duration does not matter. The two sets of intensities are chosen with respect to the lowest intensity of 3.5×10^{14} W/cm² of Ref. [12]: the difference in ponderomotive shifts at 3.5 and 5.7×10^{14} W/cm² is approximately one photon energy. Photoelectron peaks at the two intensities are located at the same energies, only differing by one photon number. Both triplets of intensities will be used in further comparison with experimental data. Choosing these two sets of intensities separated by a ponderomotive shift of $\hbar\omega$ is motivated by the calibration of intensities in Ref. [12] using shape and peak positions of single-electron spectra of 3.5×10^{14} W/cm². For such a procedure, given the uncertainty of the shapes, peak positions remain ambiguous with respect to ponderomotive shift.

Somewhat surprisingly, for this rather simple observable the agreement is not satisfactory for either set of intensities. Strikingly, at 3.5 and 4.6×10^{14} W/cm² the predicted pronounced cutoff is not found in the experimental data. The calculations at the higher set of intensities bear more similarity to the experimental data, but agreement at the high photoelectron energies remains off by nearly an order of magnitude.

The difficulty in using single-electron spectra for intensity calibration is that the photoionization threshold shifts with intensity by one or several photon energies ($\hbar\omega = 3.14$ eV), and channel closure occurs. For example, at an intensity of 4.6×10^{14} W/cm² the 10-photon transition falls right onto the ionization threshold, and at higher intensity a minimum of 11 photons is needed for ionization. If the signal is averaged over individual photoelectron peaks, the low-energy photoelectron spectrum appears to change shape rather erratically. If individual photoelectron peaks are resolved, one should be able to reliably gauge the intensity with an ambiguity of multiples of $\hbar\omega$. To resolve that ambiguity one needs

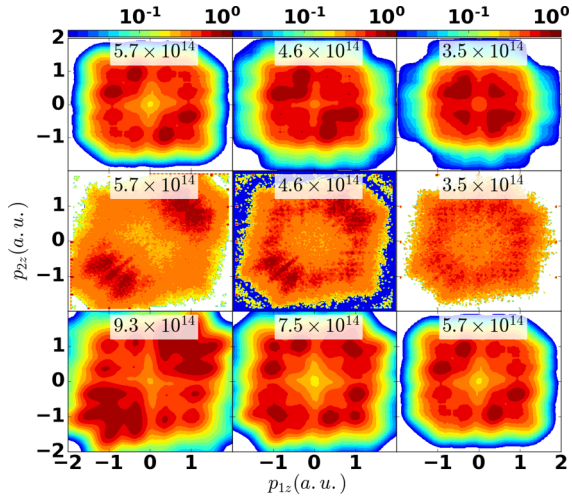


FIG. 2. First row: computed spectrum with a 394.5-nm, \cos^8 pulse. Second row: measured spectra from Ref. [12] at nominally the same intensities as the first row. Third row: computed spectra at a higher set of intensities. Computed data were smoothed for better visibility.

additional information: the checkerboard pattern observed in double emission (Sec. IV C) allows distinguishing even and odd photon counts, reducing ambiguity to multiples of twice the photon energy, $2\hbar\omega = 6.3$ eV.

The ambiguous comparison of the single-electron spectra precludes the use of these spectra for gauging the experimental intensity. The double-emission calculations below suggest that the actual experimental intensities were higher than quoted in [12].

IV. DOUBLE-ELECTRON EMISSION

A. Joint momentum distributions

In Fig. 2 we show the joint momentum distributions obtained for our two intensity sets and the corresponding data digitized from Ref. [12]. At the lower intensities from 3.5 to 5.7×10^{14} W/cm² B2B emission into the quadrants with opposite signs of the p_z momentum is more prominent. This changes markedly at 9.3×10^{14} W/cm², where the SBS emission dominates. The same transition appears in experiment, although at a nominal intensity near 5×10^{14} W/cm².

We note that the transition to dominantly SBS emission occurs at the intensities in the simulation where the energy of the recolliding electron approaches the threshold for excitation of He⁺ (cf. Ref. [27]; see also Sec. IV D). An inelastic collision at that threshold leaves both electrons at comparatively low momentum and unbound or loosely bound. From such a state, acceleration by the laser into similar directions is favored.

B. Ratio of He²⁺ to He⁺ yields

The question of experimental intensities also arises when we consider the ratio He²⁺/He⁺ of the yields of total double to single ionization. Figure 3 compares our simulations with the experimental results from Refs. [12,27]. In Ref. [27] intensities were calibrated using spot-size measurements and

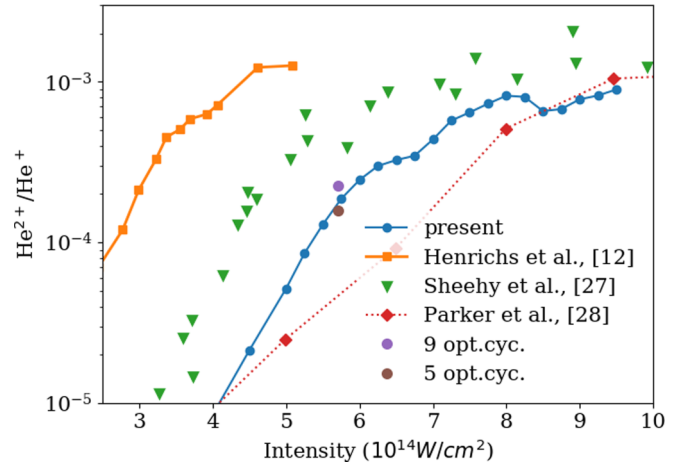


FIG. 3. He²⁺/He⁺ ratios for $\lambda = 390$ nm from the present calculation and literature values. Blue line: 7 o.c. FWHM, dots: 5 and 9 o.c. FWHM.

Xe ionization yields, with a reported uncertainty of approximately 25%. Our results suggest that the peak intensities in both experiments should be scaled to higher values, with about a factor of 2 for Ref. [12]. The discrepancy in relation to Ref. [27] was discussed in Ref. [12] considering, in particular, the shorter pulse duration used in [12]. For the bulk of our simulations we use short pulses of ~ 9 fs (7 o.c. FWHM), even shorter than in Ref. [12]. As recollision occurs within one or, at most, two optical cycles, pulse-duration effects are expected to be small and mostly due to the wider spectrum of shorter pulses. Cross-checks at an intensity of 5.7×10^{14} W/cm² show variations of $\sim 20\%$ as we change pulse duration from 5 to 9 o.c. (see Fig. 3).

Figure 3 also includes results from the *ab initio* calculation [28], which are close to our results at most intensities. In Ref. [28] yields are accumulated outside a finite radius, which is, in spirit, comparable to the present tSURFF calculation, but it differs in the use of flat-top pulses and the actual extraction method, which plausibly accounts for the observed differences.

C. The checkerboard pattern

An interesting observation reported in Ref. [12] is the appearance of a “checkerboard” pattern in the energy distributions. In Fig. 4 we show joint energy spectra at two different intensities and line-outs of the spectrum along the 40- and 48-photon peaks according to Eq. (12) for B2B and SBS events separately. The line-outs highlight the modulation of the yield at energy differences $|E_1 - E_2| = 2n\hbar\omega$. In the line-out for the higher intensity of 5.7×10^{14} W/cm² and 48 photons, modulation becomes weaker in the SBS events but remains pronounced in B2B. These observations are consistent with Ref. [12], where the pattern was observed only in B2B and became washed out with intensity, although at nominally lower intensities.

In the absence of interaction a trivial checkerboard pattern would appear in the emission of two electrons whenever there are photon peaks in the emission of the individual electrons. This cannot be the primary cause for the pattern observed

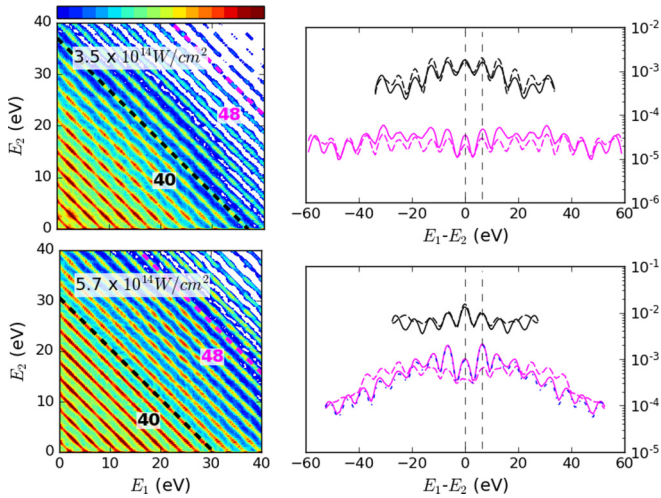


FIG. 4. Modulation of two-electron emission by the photon energy. Left: $\sigma(E_1, E_2)$ for intensities 3.5 and $5.7 \times 10^{14} \text{ W/cm}^2$ for a flat-top pulse with $\text{FWHM} = 14$ o.c. Right: line-outs at 40 (black upper lines) and 48 (magenta lower lines) absorbed photons. Solid line is for B2B, dashed is SBS, vertical dashed lines indicate two-photon spacing, and $\sigma(E_1, E_2)$ are normalized to a maximum of 1. The bottom right panel also includes the modulation for $\phi_{\text{CEP}} = \pi/2$ (dotted blue line), which nearly coincides with the result for $\phi_{\text{CEP}} = 0$ (solid magenta line).

here, as independent (“sequential”) emission of the electrons is several orders of magnitude less intense than the recollision-induced double emission. In general, periodicity of emissions modulates energy patterns at multiples of the photon energy, which is interpreted as photon counts and energy conservation, Eq. (12). In double emissions this leads to distinct photon peaks in total energy, when contributions from subsequent optical cycles add constructively. The checkerboard pattern shows that the energy *difference* favors multiples of *twice* the photon energy, $E_1 - E_2 = 2n\hbar\omega$. This is the signature of a process that occurs repeatedly at $1/2$ of the optical period. As it appears in the two electrons’ relative energy, it suggests repeated exchanges of energy between them at a time separation of $1/2$ optical period. With recollision as the main mechanism for double ionization at the given parameters, we interpret the modulation as a signature of multiple collisions of the electrons during the ionization process. Such multiple recollisions were suggested for double ionization [6–8], being more dominant at lower energies and favoring B2B emission. The energy modulation shown in Fig. 4 supports these classical predictions. The fact that the pattern appears in experiment in B2B but not in SBS emission [12] also fits the picture. The checkerboard pattern is not qualitatively affected by the exact value of ϕ_{CEP} (see Fig. 4).

D. Correlation and Freeman resonances

Figure 5 shows the correlation ratio Γ , Eq. (7), and the total double-ionization yields for intensities from 2.5 to $7 \times 10^{14} \text{ W/cm}^2$. In both curves we see peaks when the lowest excited energies $E^{(x)}$ shift into a Freeman resonance, Eq. (10). The curves are calculated with a 9 o.c. ~ 12 fs flat-top pulse. A few additional points were calculated with a pulse duration

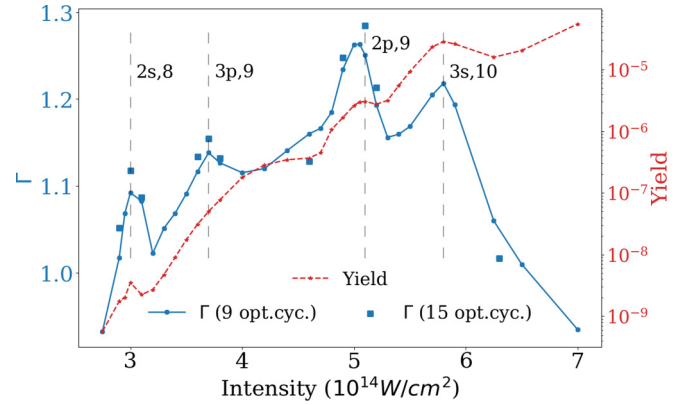


FIG. 5. Correlation ratio Γ and total DI yield as a function of laser intensity. Solid line: Γ for 9 o.c., dots: 15 o.c., dashed line: DI yield. The vertical dashed lines labeled by nl, N indicate the N -photon Freeman resonance positions with the nl state. A flat-top pulse was used.

of 15 o.c.: Γ is further enhanced, and while it drops slightly off resonance, that is to be expected.

An overview of the dependence of Γ_η on the photoelectron energies for four different intensities is shown in Fig. 6. We see that, in general, points of nonequal energy sharing are more B2B, $\Gamma_\eta > 1$. This TDSE result supports the prediction of preferred B2B emission at nonequal energy sharing [7,8] based on the analysis of classical trajectories. The classical simulations were interpreted by taking into account the modification of the classical potential by the simultaneous action of the reapproaching electron and the laser field. In more quantum-mechanical language this is excitation simultaneous with tunneling and/or over barrier ionization. The mechanisms are distinguished from the conventional idea of RESI

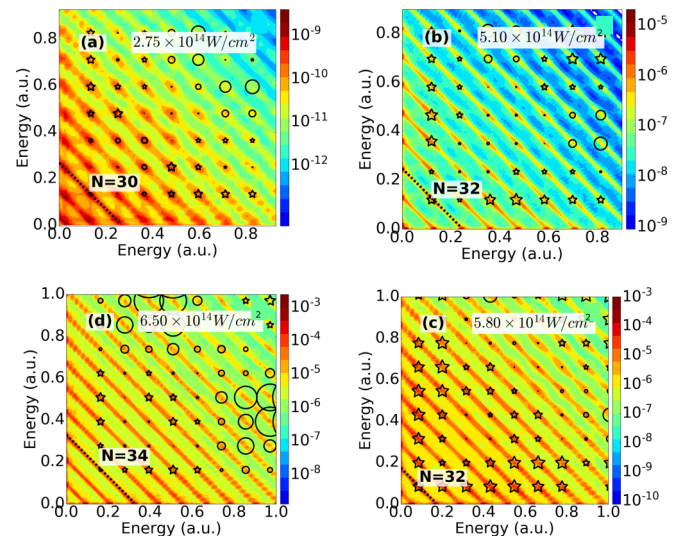


FIG. 6. Joint energy distributions for four different intensities. Circles indicate more SBS emission, $\Gamma_\eta < 1$; stars indicate more B2B, $\Gamma_\eta > 1$ at $\eta = (E_1, E_2)$; and the size of the symbols indicates the pronouncement of the effect. Panels (a) and (b) are without Freeman resonance and (b) and (c) on resonance (see also Fig. 5). The black lines labeled by N indicate N -photon energy peaks in $E_1 + E_2$.

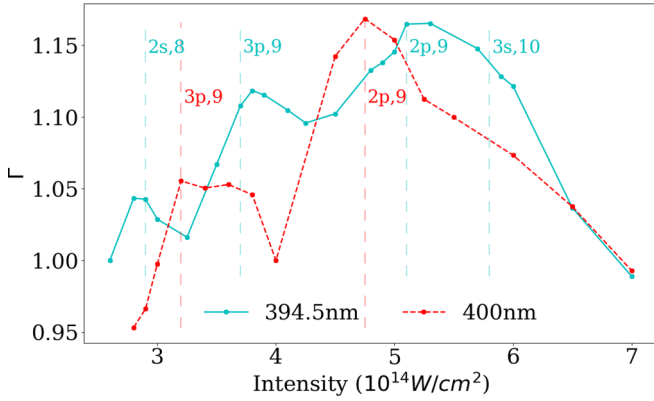


FIG. 7. Correlation ratio Γ as a function of laser intensity with a \cos^8 pulse, FWHM = 7 o.c. pulse with λ at 394.5 and 400 nm. The vertical dashed lines labeled by nl, N indicate the N -photon Freeman resonance positions with the given excited state at the respective wavelength.

in that excitation and ionization happen within the time frame of a given recollision. In contrast, in RESI the two single ionizations would ultimately occur without narrow correlation in time and would leave emission directions largely independent.

A more precise mapping of the mechanisms onto quantum mechanics is difficult: both the presence of a rather strong field and the brevity of the interaction deprives individual states of their identity. Wave functions can, with great success, be associated with trajectories at larger distances from the nucleus, but the mapping breaks down as one approaches the range of the electrons' de Broglie wavelengths. Still, the behavior of B2B emission corroborates the essence of Refs. [7,8]: the contribution from DUR is important, in addition to a possible RESI background.

Figure 5 was computed with flat-top pulses for better exposure of the mechanism, but Freeman peaks in B2B emission also appear with the more realistic \cos^8 pulse envelope, as shown in Fig. 7.

Freeman resonances do not appear in classical simulation, as they depend on the quantization of excitation energies. Resonance implies, in particular, that there is a well-defined photon energy and that the process spans several optical periods. In such a mechanism, standard multiphoton-type excitation is followed by double ionization from the excited state. The fact that Freeman resonances enhance B2B emission indicates that that mechanism is of the DUR type.

E. Joint angular distributions

JADs strongly depend on the total energy, the energy sharing between the two electrons, and the laser parameters. Figure 8 reproduces two JADs from Ref. [12] together with our results. For illustration we have chosen two points with equal energy sharing $E_1 = E_2$ at 5.5 and 8.8 eV. Experiment and simulation agree in showing clear angular anticorrelation. Near an intensity of $3.5 \times 10^{14} \text{ W/cm}^2$, the JAD bends into the lower half plane, away from the first emitted electron. At the higher intensity of $5.7 \times 10^{14} \text{ W/cm}^2$ anticorrelation is less pronounced, and shapes are more similar to the experimental ones. Apart from that general qualitative behavior, the spectra vary significantly with the exact pulse shape and intensity. Because of the high sensitivity to intensities, e.g., comparing 3.5 and $3.7 \times 10^{14} \text{ W/cm}^2$, a more detailed comparison of computed JADs with experiment is not possible at this point.

By studying the convergence with increasing R_s we see that the bulk of correlation effects originates at distances $\lesssim 30$ a.u. from the nucleus. Figure 9 shows the convergence of the correlation ratio Γ and the maximal relative error of the energy-integrated angular distributions

$$\epsilon_{\text{JAD}} = \max_{\theta_1, \theta_2} \frac{|\sigma(\theta_1, \theta_2) - \sigma^n(\theta_1, \theta_2)|}{\sigma(\theta_1, \theta_2)}, \quad (13)$$

where σ^n refers to results obtained with the next smaller box size. While Γ is converged for the purposes of the present argument, convergence of the JADs remains delicate, but qualitatively correct results may be expected at interaction ranges $R_s \gtrsim 40$.

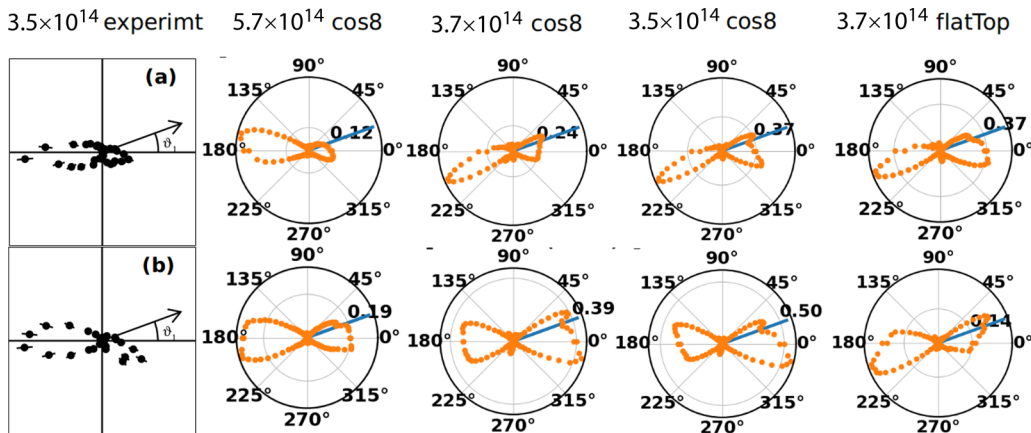


FIG. 8. JADs from Ref. [12] (leftmost) and present simulations at energies $E_1 = E_2 = 5.5$ eV (top row) and 8.8 eV (bottom row). The direction of the first electron (blue lines) is fixed at $\theta_1 = \pi/6$ relative to the polarization axis. Intensities and pulse shapes are indicated above the respective columns. The distributions are averaged over $\pm 4^\circ$ and normalized to a maximal emission of 1. A flat-top pulse (last column) does significantly, but not qualitatively, change the JAD.

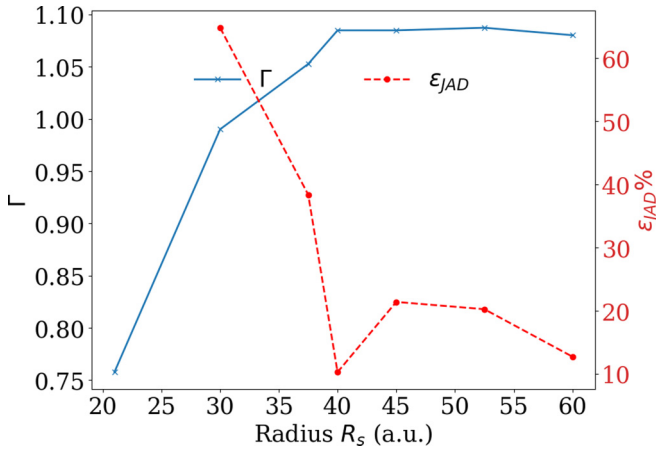


FIG. 9. Convergence of Γ and JADs with the radius R_s of the interaction region. Calculations are at 5×10^{14} W/cm² and a FWHM of 2 fs. ϵ_{JAD} is the maximal relative error of the JADs, Eq. (13).

F. Double-emission by short pulses

We also investigated double emission by extremely short pulses of 2 fs FWHM with the purpose of identifying a signature of the “slingshot” mechanism for B2B emission which was proposed in [3]. In that mechanism, the first electron’s momentum changes sign in a close encounter (slingshot), while the second electron is emitted with some delay that results in B2B emission. Reference [3] reported pronounced B2B emission at a pulse duration of 2 fs and intensity 5×10^{14} W/cm² as a signature of the mechanism. Figure 10 compares that classical finding with our TDSE simulations. The result for 5×10^{14} W/cm² favors unequal energy sharing, which is characteristic of a DUR process. In contrast, the 3×10^{14} W/cm² result bears great similarity to the classical simulation with more weight on equal energy sharing.

While our finding does not rule out the slingshot mechanism at 5×10^{14} W/cm², it indicates important double ionization through alternative pathways with unequal energy sharing. Note that we use the exact same pulse as in Ref. [3].

The slingshot mechanism may be dominating at the lower intensity. However, attempts to trace the classical motion of the two electrons while studying time-dependent spatial correlations in the quantum wave function failed due to the general difficulty of such a mapping. In addition, we remark that the

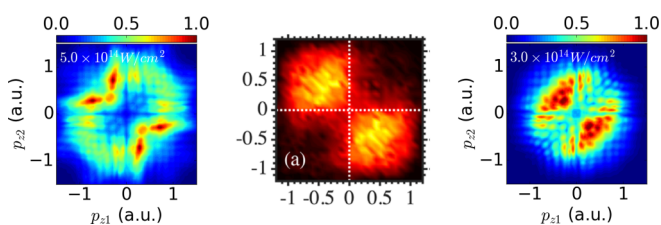


FIG. 10. Joint momentum distributions in the p_z direction at FWHM = 2 fs and intensity averaged over the carrier-envelope phase. Middle: classical trajectory calculation at 5×10^{14} W/cm², reproduced from Ref. [3] [Fig. 1]. Left: TDSE result for 5×10^{14} W/cm²; right: TDSE for 3×10^{14} W/cm². Densities are normalized to a maximal value of 1.

very large bandwidth of the 2-fs pulse admits lower-order multiphoton ionization, which erodes the quasistatic tunneling picture employed for initial ionization in the classical model. Also, by their very construction, classical calculations do not account for effects of the quantum-mechanical structure of the atom, for example, the Freeman resonances discussed above.

V. CONCLUSIONS

The *ab initio* quantum-mechanical calculations of single and double emissions confirm the generally important role of DUR-type double ionization, where the second ionization is simultaneous with the recollision if we accept the enhancement of B2B emission as a signature of the process. This is supported also by the relatively stronger B2B emission at spectral points with large differences between electron energies. Further differentiation of the classical mechanisms is hampered by the fact that Freeman resonances add a genuine quantum aspect to the discussion and that the individual classical mechanisms involve concepts such as classification of individual trajectories or exact release times, for which at present no quantum correspondence exists.

In a comparison with recent experimental results on double-emission spectra [12], we find good qualitative agreement if we allow for an increase in experimental intensities by a factor of ~ 2 . Such an adjustment is suggested by three different and largely independent observables: the He²⁺/He⁺ ratio, the dependence of B2B emission on intensity, and the intensity where the checkerboard pattern in joint energy distributions fades.

Unfortunately, the ambiguity of intensity could not be resolved using the single-electron spectra published in [12]: this observable can be computed easily and with great reliability, but we were unable to establish convincing agreement at any set of intensities. Again, intensities higher than the experimental ones appear to be favored.

We have not considered volume averaging over intensities when comparing them to the experimental results. One reason is that the experimental arrangement of Ref. [12] managed to strongly reduce the effect by collimating the atomic beam, which makes contributions from half of the peak intensity appear unlikely. Also, averaging effects would exacerbate the disagreement with experiment, as even higher peak intensities would be needed to achieve a given yield. In general, considering the near-exponential drop of yields at our lower intensities (see Fig. 3), we expect only minor effects from volume averaging, mostly by Stark-induced broadening and displacement of the peaks. Such effects should be reexamined when detailed experimental data become available.

For JADs we can clearly identify the effect of electron repulsion, analogous to what was reported in [12]. Comparison with experiment beyond that general level is made difficult by the sensitivity of the JADs to intensity, carrier-envelope phase, pulse duration, and exact pulse shape. On the computational side, for reliable convergence of JADs one needs to take into account the interaction between electrons over large spatial regions, which inflates tSURFF computations to large scale.

Finally, we offer a simple explanation for the checkerboard pattern noted in [12], which also appeared in earlier

simulations at 800 nm [22]: the modulation at energy differences of $2\hbar\omega$ means that the underlying process involves periodic reencounters of the two electrons at one half of the optical period, i.e., multiple recollisions.

ACKNOWLEDGMENTS

J.Z. was supported by the DFG Priority Programme 1840, QUTIF. We are grateful for fruitful discussions with G. Katsoulis, A. Emmanouilidou, K. Henrichs, and R. Dörner.

-
- [1] B. Walker, B. Sheehy, L. F. DiMauro, P. Agostini, K. J. Schafer, and K. C. Kulander, *Phys. Rev. Lett.* **73**, 1227 (1994).
 - [2] J. Ullrich, R. Moshhammer, A. Dorn, R. Dörner, L. P. H. Schmidt, and H. Schmidt-Böcking, *Rep. Prog. Phys.* **66**, 1463 (2003).
 - [3] G. P. Katsoulis, A. Hadjipittas, B. Bergues, M. F. Kling, and A. Emmanouilidou, *Phys. Rev. Lett.* **121**, 263203 (2018).
 - [4] A. Vilà, J. Zhu, A. Scrinzi, and A. Emmanouilidou, *J. Phys. B* **51**, 065602 (2018).
 - [5] H. Price, C. Lazarou, and A. Emmanouilidou, *Phys. Rev. A* **90**, 053419 (2014).
 - [6] Y. Liu, S. Tschuch, A. Rudenko, M. Dürr, M. Siegel, U. Morgner, R. Moshhammer, and J. Ullrich, *Phys. Rev. Lett.* **101**, 053001 (2008).
 - [7] S. L. Haan, Z. S. Smith, K. N. Shomsky, and P. W. Plantinga, *J. Phys. B* **41**, 211002 (2008).
 - [8] D. F. Ye and J. Liu, *Phys. Rev. A* **81**, 043402 (2010).
 - [9] S. L. Haan, L. Breen, A. Karim, and J. H. Eberly, *Phys. Rev. Lett.* **97**, 103008 (2006).
 - [10] T. Shaaran, M. T. Nygren, and C. Figueira De Morisson Faria, *Phys. Rev. A* **81**, 063413 (2010).
 - [11] A. Emmanouilidou, J. S. Parker, L. R. Moore, and K. T. Taylor, *New J. Phys.* **13**, 043001 (2011).
 - [12] K. Henrichs, S. Eckart, A. Hartung, D. Trabert, K. Fehre, J. Rist, H. Sann, M. Pitzer, M. Richter, H. Kang, M. S. Schöffler, M. Kunitski, T. Jahnke, and R. Dörner, *Phys. Rev. A* **98**, 043405 (2018).
 - [13] A. Scrinzi, tRecX, <https://trex.physik.lmu.de>.
 - [14] A. Scrinzi, *New J. Phys.* **14**, 085008 (2012).
 - [15] L. Tao and A. Scrinzi, *New J. Phys.* **14**, 013021 (2011).
 - [16] C. Hofmann, A. S. Landsman, A. Zielinski, C. Cirelli, T. Zimmermann, A. Scrinzi, and U. Keller, *Phys. Rev. A* **90**, 043406 (2014).
 - [17] A. Karamatskou, S. Pabst, Y. J. Chen, and R. Santra, *Phys. Rev. A* **89**, 033415 (2014); **91**, 069907(E) (2015).
 - [18] L. Yue and L. B. Madsen, *Phys. Rev. A* **90**, 063408 (2014).
 - [19] V. P. Majety, A. Zielinski, and A. Scrinzi, *New J. Phys.* **17**, 63002 (2015).
 - [20] V. P. Majety, A. Zielinski, and A. Scrinzi, *J. Phys. B* **48**, 25601 (2015).
 - [21] L. Torlina, F. Morales, J. Kaushal, H. G. Muller, I. Ivanov, A. Kheifets, A. Zielinski, A. Scrinzi, S. Sukiasyan, M. Ivanov, and O. Smirnova, *Nat. Phys.* **11**, 503 (2014).
 - [22] A. Zielinski, V. P. Majety, and A. Scrinzi, *Phys. Rev. A* **93**, 023406 (2016).
 - [23] C. W. McCurdy, M. Baertschy, and T. N. Rescigno, *J. Phys. B* **37**, 17 (2004).
 - [24] A. Scrinzi, *Phys. Rev. A* **81**, 053845 (2010).
 - [25] T. N. Rescigno and C. W. McCurdy, *Phys. Rev. A* **62**, 032706 (2000).
 - [26] R. R. Freeman, P. H. Bucksbaum, H. Milchberg, S. Darack, D. Schumacher, and M. E. Geusic, *Phys. Rev. Lett.* **59**, 1092 (1987).
 - [27] B. Sheehy, R. Lafon, M. Widmer, B. Walker, L. F. DiMauro, P. A. Agostini, and K. C. Kulander, *Phys. Rev. A* **58**, 3942 (1998).
 - [28] J. S. Parker, L. R. Moore, D. Dundas, and K. T. Taylor, *J. Phys. B* **33**, L691 (2000).